Journal of Magnetism and Magnetic Materials 466 (2018) 186–191

Contents lists available at ScienceDirect

Journal of Magnetism and Magnetic Materials

journal homepage: www.elsevier.com/locate/jmmm

Research articles

Evolution of surface antiferromagnetic Néel temperature with film coverage in ultrathin MnO films on Ag(001)

Asish K. Kundu[a,b,*], Sukanta Barman[a,c], Krishnakumar S.R. Menon[a]

[a] Surface Physics and Material Science Division, Saha Institute of Nuclear Physics, HBNI, 1/AF Bidhannagar, Kolkata 700064, India
[b] International Center for Theoretical Physics (ICTP), I-34014 Trieste, Italy
[c] Department of Physics, Raja Peary Mohan College, Uttarpara, Hooghly 712258, India

ARTICLE INFO

Keywords:
Oxide thin film
Surface magnetism
LEED
Critical exponent

ABSTRACT

The surface antiferromagnetic ordering of MnO(001) ultrathin films has been probed using Low-energy Electron Diffraction (LEED) and Angle-Resolved Photoemission spectroscopy (ARPES) techniques. We observe coherent exchange scattered half-order spot in LEED which is only visible at low electron beam energy (<40 eV) and arises below a certain temperature with a periodicity of the magnetic unit cell of MnO(001) surface, confirms its magnetic origin. A thickness dependent evolution of surface antiferromagnetic (AFM) Néel temperature has been observed for the MnO films. Interestingly, we found the Néel temperature of the MnO films exceed its bulk Néel temperature even in the ultrathin limit (~2 ML). Detailed LEED analysis reveals that the increase of the Néel temperature is due to the presence of strain and the image charge screening effect in the film while, the competition between the finite size effects, surface strain, and substrate polarizability ultimately determine the observed Néel temperature. The surface magnetic critical exponent (β_1) varies from $0.16 \pm .03$ to $0.81 \pm .03$, upon changing film thickness from 3 to 10 ML, indicates the transition from nearly 2D Ising system to 3D Ising/Heisenberg system. Furthermore, upon paramagnetic (PM)-AFM transition, ARPES energy distribution curves (EDCs) show, opening an energy gap of 150 meV with an increased occupation in the e_g levels is good agreement with the theoretical prediction of the presence of AFM-II type ordering in the film.

1. Introduction

The bulk magnetic 3*d* monoxides (MO; M = Ni, Co, Mn) with rock-salt structure (NiO, CoO, MnO) are the well known antiferromagnetic insulators. The antiferromagnetism of these oxides are well understandable from the superexchange mechanism which occurs through the M-O-M network. The bulk magnetic properties of many binary (NiO, CoO, MnO) or complex oxides (Cr_2O_3, Mn_3O_4, $BaTiO_3$, etc.) have been rigorously studied over the past few decades while the surface properties even for the simple binary oxides are lacking in literatures [1–3]. The reason could be the lack of availability of high-quality oxide surfaces to obtain reproducible results, as the cleaved surface of oxide single crystals are often shows poor structural quality. Another problem is that most of these oxides are highly insulating which create difficulties in electron spectroscopic measurements [4–6]. Among transition metal oxides, MnO shows highest value of local magnetic moment ~ $5\mu_B$, thus, could be a model system to study the spin-dependent properties. However, for the case of MnO single crystal, where the cleavage along the (001) plane normally leads to a surface, which consists of pyramids with (111) octahedral faces along with (001) [7]. These issues can be overcome by making thin films of MnO on a suitable metallic substrates. Further, in case of thin films, we may also expect the possibility of emerging new electronic and magnetic properties due to confinement in a thin layer. Thus, it could be interesting to study the magnetism of MnO in ultrathin film regime.

Although, there are many techniques available to measure bulk antiferromagnetism, only a few techniques (SP-STM, XMLD-PEEM, etc) [8–10] are available which can probe antiferromagnetism in the ultrathin film region. Recently, Batanouny et al. [11] has used Metastable Helium Ion Scattering techniques to the NiO(001) and CoO(001) surface to find out the surface antiferromagnetic structure. Long time back, Palmberg et al. [12] had first used LEED as a technique to detect surface antiferromagnetism of NiO(100). They have observed half order spot in LEED, produced by exchange scattered low energy electrons, with (2×1) translation symmetry from the antiferromagnetic NiO below the Néel temperature (T_N). They have also mentioned, as exchange interaction is very small than Coulomb interactions, the intensity of these spots will be very small. After that, our group is using this techniques

* Corresponding author presently at: International Center for Theoretical Physics (ICTP), I-34014 Trieste, Italy.
E-mail addresses: asishkumar2008@gmail.com (A.K. Kundu), krishna.menon@saha.ac.in (K.S.R. Menon).

https://doi.org/10.1016/j.jmmm.2018.07.005
Received 9 April 2018; Received in revised form 26 June 2018; Accepted 4 July 2018
Available online 05 July 2018

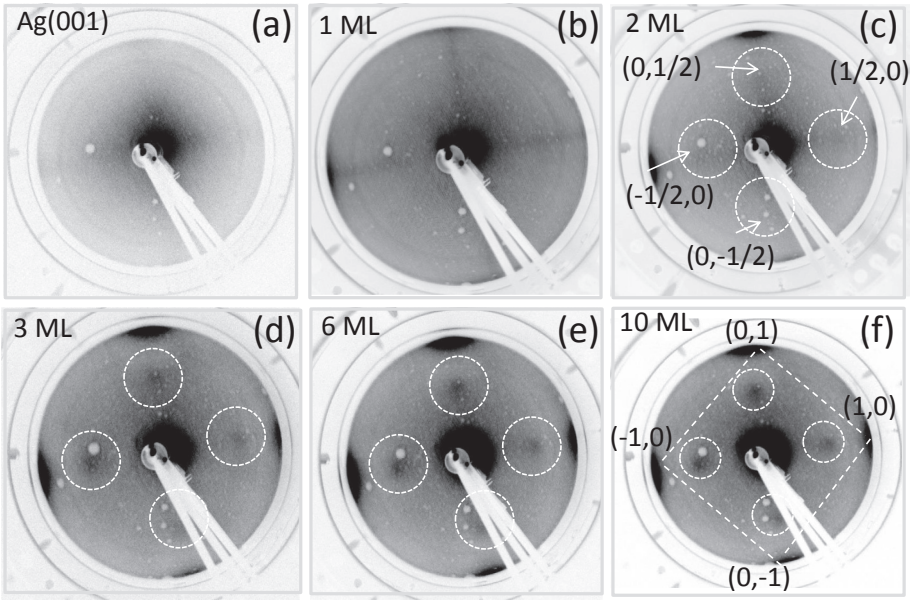

Fig. 1. LEED images (reverse contrast) at primary electron beam energy (E_P) of 20 eV and at LN_2 temperature (108 K) from (a) clean Ag(0 0 1) substrate and MnO film thickness of (b) 1 ML (c) 2 ML (d) 3 ML (e) 6 ML (f) 10 ML. Dotted circles represent the half order spot positions and the square shape dotted line shows the $p(1 \times 1)$ unit cell of MnO(0 0 1).

extensively for different antiferromagnetic system like NiO/Ag(001) [10], 1 ML Cr/Ag(0 0 1) [13,14], etc, as a probe of surface antiferromagnetism.

Not only the surface antiferromagnetic ordering but also more other valuable information can also be obtained from the temperature variation of the exchange scattered half order spot intensity, like, in-plane and out-of-plane exchange parameter [15] as well as Néel temperature of the surface/ultrathin films [14,15]. Further, the critical exponent of the sublattice magnetization (β) can be obtained from the fitting of the temperature dependence of the square root of half order intensity variation data with the universal power law of the sublattice magnetization, $M_S(T) \sim (1-T/T_C)^{\beta}$ [16]. Although, there are many physical and technological importance of transition metal oxides, as per our knowledge, only one experimental report by Hermsmeier *et. al.* [17] is available in the literature for the study of the magnetism of MnO(001) surface. Where they have basically shown the presence of short-range AFM order above T_N for MnO(001) surface using Spin-Polarized Photoelectron Diffraction (SPPD) technique. Only a few growth and structural characterization papers of MnO(100) surface is available in the literature [6,18–21] as maximum attention was paid to the NiO/Ag (001) and NiO/Ni(001) systems [22–24].

In this paper, we probe the surface antiferromagnetic ordering of MnO(001) ultrathin films by LEED technique. This is the first experimental report from MnO(001) ultrathin film system, where we observed the evidence of antiferromagnetism even in the ultrathin film (~2 ML) region. Evolution of the surface antiferromagnetic Néel temperature with film thickness is explored. We observe the enhancement of Néel temperature at the surface of ultrathin film than bulk MnO even in the case of ~2 ML MnO on Ag(001) which cannot be explained only by considering the superexchange interactions, even though the Néel temperature for the bulk antiferromagnetic oxides is well understood in terms of the superexchange interactions. We have shown a combination of superexchange interaction, finite size effects, and image charge screening effect can explain the observed Néel temperature variation quite well. The variation of surface magnetic critical exponent (β_1) upon film thickness has been explained using Ising and Heisenberg model. We have also shown how the antiferromagnetic ordering affects the valence band electronic structure of MnO.

2. Experimental details

Epitaxial MnO films have been grown on Ag(001) single crystal substrate, prepared by standard cycles of Ar^+ ion sputtering (600 eV, 1 μA) for 15 min followed by UHV annealing at 773 K for 30 min until a sharp $p(1 \times 1)$ is observed. During the experiment, the base pressure of the preparation chamber was 1×10^{-10} mbar. High purity Manganese (99.99%) was evaporated from a well-degassed water cooled e-beam evaporator at a constant rate of 0.3 Å/min, in oxygen environment (1×10^{-8} mbar). The details of growth procedure for the well-ordered MnO can be found from our previously published work [25,26]. Sample temperature was measured by a K-type thermocouple, in contact with the Ag(001) crystal. The crystalline quality of the films were determined by a four-grid LEED apparatus (OCI Vacuum Microengineering) attached to the preparation chamber. A highly-sensitive Peltier-cooled 12-bit CCD camera was used to collect LEED images. The gain/exposure settings of the camera and different controls of the LEED instrument has been performed with the software control through the computer. ARPES measurements were performed *in situ* inside analysis chamber using a combination of VG SCIENTA-R4000WAL electron energy analyzer with a 2D-CCD detector and a high flux GAMMADATA VUV He lamp attached with a VUV monochromator, having base pressure better than 8×10^{-11} mbar. The details of the instrumental setup have been described in detail elsewhere [27]. He II_α (40.8 eV) resonance line has been used as an excitation for ARPES measurement which has an energy resolution better than 0.1 eV, including the thermal broadening near E_F at room temperature.

3. Experimental results and discussions

3.1. Magnetism of the MnO(001)/Ag(001) system

It is well-known that the bulk MnO is an antiferromagnetic insulator with an Néel temperature of 122 K but what about the magnetism at the surface of the MnO(001) ultrathin film? To elucidate, if there is any evidence of antiferromagnetism in the ultrathin MnO(001) films, we have cooled down the well-ordered $p(1 \times 1)$ MnO(001) sample, keeping under the LEED screen. During cooling, after a critical temperature, a few extra spots [see Fig. 1(c)-(f)] arises in the midway

position between (0,0) spot and the (1 × 1) spots and these extra spots are only visible in the low electron beam energy (12–35 eV). We called these spots as half-order spot as it arises in the midway position between (0,0) spot and the (1 × 1) spots. Appearance of these extra spots could be due to the presence of magnetic $p(2 \times 1)$ twin domain structure, similar to the case of NiO [12]. Fig. 1(a), shows the LEED image of a clean Ag(001) surface at 20 eV electron beam energy. We did not find any spots in the image [see Fig. 1(a)], as the first order diffraction spots are out of the field-of-view due to the low energy of the electron beam. Fig. 1(b)-(f), represents the LEED images of the 1 ML, 2 ML, 3 ML, 6 ML and 10 ML film coverages of MnO, which are taken at liquid nitrogen (LN^2) temperature (108 K) with a primary electron beam energy of 20 eV. LEED images are taken at 20 eV energy to get the maximum intensity of the exchange scattered spots. For 1 ML MnO/Ag(001), we do not observe any distinct spots in the LEED images at 20 eV, but only find weak line stripes connecting (0, 0) spots with the integer order spot. These stripes are likely due to the strain-induced mosaic pattern of the film as there is 8% lattice mismatch between Ag and MnO. But for 2 ML MnO, we find faint and broad intensity arising in the half-order spot positions, indicated by the circular white dotted circle in the Fig. 1(c), and these spots are prominent for the higher film thickness. The intensity of these half-order spots are only (2%–3%) of the integer order spots. The appearance of these extra spots can be explained easily by the magnetic unit cell structure of MnO, similar to the case of NiO. Schematic diagram of the magnetic unit cell of MnO is shown in the Fig. 2(a), where the arrangement of Mn^{2+} ions in a magnetic unit cell of MnO are shown. In MnO crystal, magnetic moments are aligned parallel within (111) planes and is antiparallel between adjacent planes [28]. The red and black arrow shows the spin directions between two consecutive (111) planes. Spin arrangements of the MnO(001) surface are shown in Fig. 2(b). It is clear that the spin arrangement of the MnO (001) surface has a $p(2 \times 1)$ translation symmetry with respect to the chemical unit cell of the MnO. Thus, if low energy electrons fall on the MnO(001) surface then the scattered electrons from the $p(2 \times 1)$ magnetic unit cell of MnO, are expected to show $p(2 \times 1)$ twin-domains structure. Due to the fourfold symmetry of the surface of MnO(001), twin-domains appear in LEED at the right angle to each other. But, the problem is that the occurrence of the twin domains (half-order) spots in LEED can be due to the structural or magnetic origin. But, structural spots can be separated from the magnetic spots by examining a few properties of these spots. The structural half-order spots should be seen at any electron beam energy with an intensity comparable to the integer order spots, as both spots originating from the Coulomb scattering. Further, the intensity of the structural half-order spots should not change much with the temperature. In order to rule out the possibility of structural half order spots in our experiment, we have checked how the half-order spot intensity varies with the incident electron beam energy (see Fig. 3). From Fig. 3, it is clear that the intensity of the (1/2,0) spot is maximum at 20 eV and then decreases with increasing electron beam energy and further increase at 29 eV and beyond that no peaks can be identified. The poor statistics for the measured I-V curve in Fig. 3 is due to the weak intensity of the half-order spots. These peaks at 20 and 29 eV are originating due to the formation of antiferromagnetic twin-domain structure. Because, each half-order spot visible in LEED is composed of the normal projections from the two magnetic reciprocal lattice points separated by their k_z coordinates [29,30]. With the variation of electrons kinetic energy, we are mainly sensitive to the different k_z planes in the reciprocal space. Thus, we are sensitive to the two different magnetic twin domains in those two-particular energies. Similar variation of the (1/2,0) spot intensity with the electron beam energy has also reported for prototypical system, e.g., NiO, where their origin could successfully be interpreted in terms of antiferromagneic twin-domain structure [10,30]. In fact, for the NiO(001), these twin-domains are fully resolved from the dark-field LEEM images taken at these two energies where the half-order LEED-IV shows maximum intensity [30]. On the other hand, a typical temperature dependence of these spots (see Fig. 4), occurs below a certain critical temperature with the intensity of the spots only (2%–3%) of the integer order spots and only visible at low electron beam energies (<35 eV), confirms its antiferromagnetic origin. It is only visible at low electron beam energies because the cross-section of exchange scattering decreases sharply with increasing electron beam energy [12]. A rough estimation of the average antiferromagnetic domains size can be obtained from the full width at half maximum (FWHM) of the half-order spots [20,31]. The estimated average domain size for 10 ML MnO film is about 6 nm.

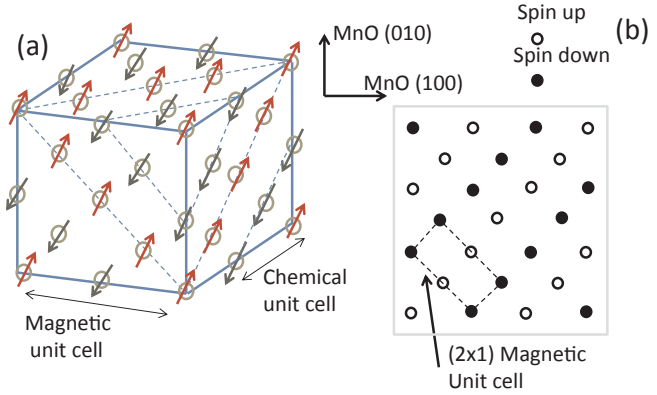

Fig. 2. schematic diagram of the arrangements of Mn^{2+}(sphere) in the MnO. The O^{2-} ions are not shown in the figure. In each (111) planes, magnetic moments are aligned parallel to the plane and it is antiparallel between consecutive (111) planes. Where red and black arrow represents the spin directions between two consecutive (111) planes. (b) Shows the Arrangements of Mn^{2+} ions in the MnO(100) surface. Where the black filled and open circles represent the spin down and spin up respectively. The dotted rectangle in Fig. 2(b) represents the (2 × 1) magnetic unit cell.

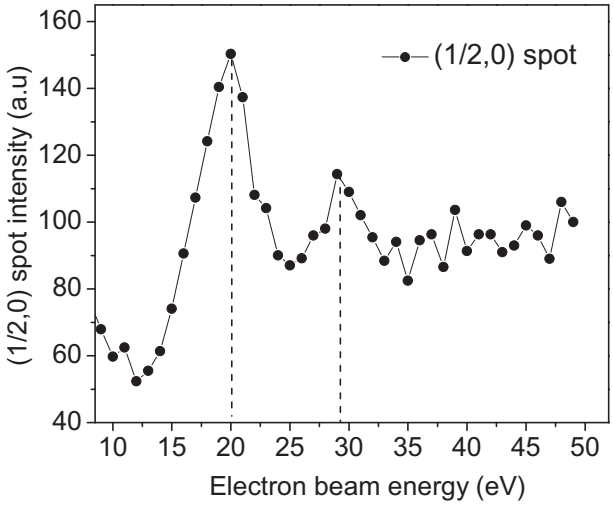

Fig. 3. Intensity variation of the half order spot with a primary electron beam energy (Ep). At Ep = 20 eV, the half order spot intensity is maximum.

The Néel temperature of the films can be estimated from the temperature dependence of the half-order spots intensity plot [12]. Generally, LEED spots intensity are known to decrease with increasing temperature due to the thermal motion of atoms (i.e., lattice vibration). According to the single scattering theory, the intensity is reduced by the Debye–Waller factor e^{-2W}, where W is proportional to temperature T [32]. The Debye–Waller factor was calculated from the temperature dependence of the specular spot intensity, similar way as reported by Hanf et al. [16]. The variation of the normalized half-order spots intensity (i.e., the intensity of the half-order spot is divided by its highest intensity) with temperature has been plotted for the different film

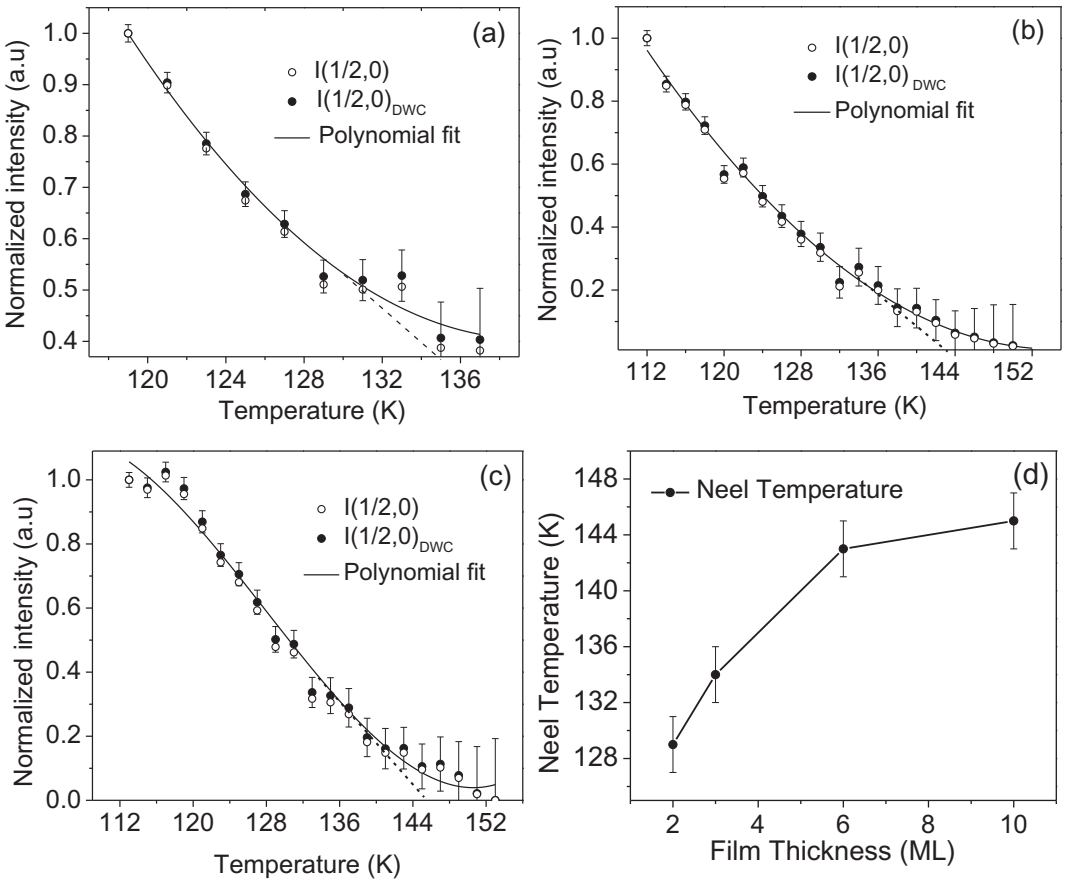

Fig. 4. Temperature dependence of (1/2,0) spot intensity for (a) 3 ML, (b) 6 ML, (c) 10 ML film thickness. The open circles correspond to the background subtracted (1/2,0) spot intensity and solid circles are after Debye–Waller factor correction. (d) Shows the variation of Néel temperature with film thickness with an error bar of ~ ±2 K.

thickness of MnO in Fig. 4(a)-(c). The open and the solid circles represent the intensity of the half-order spot before and after Debye–-waller factor correction, respectively. The continuous line is the polynomial fitted curve after Debye–Waller factor correction. We do not observe much effects of the Debye–Waller factors in our experiment as the lattice vibration effects are expected to be very less in our measured temperature ranges, 108 to 155 K.

In Fig. 4(a) to (c), the temperature above which the intensity of the half-order spot vanishes is defined as the surface Néel temperature of the film, similar to the reported by Palmberg et al. [12]. The surface Néel temperature is estimated from the cutting point of the tangent (dotted line) to the temperature axis. Fig. 4(d) shows the variation of the Néel temperature of MnO with the film thickness. No temperature dependence data has been shown for 2 ML film thickness due to the faint intensity of the half-order spots. But we have estimated the Néel temperature by looking at the LEED images and it is found to be around 129 K. From Fig. 4(d), it is clear that with increasing film thickness, the Néel temperature increases and after a certain film thickness of 6 ML it is nearly constant. This saturated value of the Néel temperature is about 23 K higher than the bulk Néel temperature of MnO (122 K). Generally, the magnetism and the Néel temperature of the simple bulk antiferromagnetic oxides are well understood in terms of superexchange interactions strength. However, the observed Néel temperature (T_N) variation in our experiment cannot be explained only by considering the simple superexchange effect (i.e., the Mn 3*d*-O 2*p* hybridization). As, Ag has 8% lower lattice parameter than MnO, thus, in the low film coverage, the MnO lattice is subjected to in-plane compressive stress [25] which increases the Mn 3*d*-O 2*p* hybridization. This increased hybridization, in turn, leads to an enhanced superexchange strength, resulting enhancement of T_N. By only considering superexchange interactions, as with increasing film thickness the surface strain relaxes, the T_N of the films is expected to decrease due to the decreased superexchange strength. However, our experimental results show just the opposite effect [see Fig. 4(d)], where the T_N is found to increase with increasing film thickness.

This variation of T_N with film thickness can be explained by taking the combined effect of the substrate induced strain and the change in the number of nearest neighbor atoms (surface coordination number) with film thickness. For low film thickness, although strain is trying to increase the superexchange interaction while due to the reduced number of nearest neighbors, it again tries to decrease the superexchange interaction. For the intermediate film thickness regime, the superexchange is dominated due to the increased number of nearest neighbors (or enhanced finite-size effects) over the strain relaxation effect, resulting increase of T_N with increasing film thickness. Our previous study [25] shows that, for 6 ML film thickness and above, most of the strain in the film has relaxed and the number of the nearest neighbors do not change much (finite-size effects are nearly saturated), leading to the near saturation of the Néel temperature (T_N).

From Fig. 4(d), it is clear that the Néel temperature for the 10 ML film is 145 K, which is 23 K more than the bulk Néel temperature value of MnO. Interestingly, even for the 2 ML MnO film the T_N is higher than the bulk T_N, which can be explained by the enhanced Mn 3*d*-O 2*p* hybridization resulting from the in-plane compressive strain. But the question still remains why the T_N of 10 ML MnO film is higher than its bulk value, despite the near-absence of strain effects and finite-size effects? This can be explained by taking into account the effect of image charge screening due to the proximity to the highly polarizable substrate Ag(001) [33]. As suggested by Altieri et al. [33], due to the proximity of a strongly polarizable medium, the superexchange

interactions, and thus the magnetic ordering temperatures can be increased by reducing the energies of the underlying virtual charge excitations as a result of the image charge like screening. We are expecting the similar effect is also applicable in our system. Thus, the superexchange strength is increased in the MnO films due to the image charge screening effect, as a result T_N of the films is increased beyond the bulk T_N. It should be noted that for the case of 1 ML MnO(001) film, we do not observe any half-order spots. The absence of the half-order spot does not mean that the film is not antiferromagnet. It is possible that the Néel temperature of the 1 ML film is lower than the measuring limit (<108 K) in our experimental setup. It will be interesting to explore the magnetism of the 1 ML MnO film and will be the subject of a future study.

Further, to understand whether the system belongs to Heisenberg/Ising or mean-field model, we have estimated the surface magnetic critical exponent (β_1) using the relation $M_S(T) = (1-T/T_N)^{\beta_1}$. As sublattice magnetization ($M_S(T)$) depends on the square-root of the exchange scattered half-ordered spot intensity, thus this equation can be written as

$$I^{1/2}(T) = (1-T/T_N)^{\beta_1}$$

$$ln(I) = 2\beta_1 ln(1-T/T_N)$$

Thus, the plot of the ln(I) *vs.* ln(1-T/T_N) will be straight line with a slope $2\beta_1$. In Fig. 5(a), the experimental plot of ln(I) *vs.* ln(1-T/T_N) for the 10 ML MnO films in the temperature ranges, 0.82–0.98 T_N is presented. The obtained value of the critical exponent for the 10 ML film is $\beta_1 = 0.81 \pm .03$. This value of critical exponent for the surface sublattice magnetization is very close to the Heisenberg model ($\beta_1 = 0.81$) [34] and 3D Ising model ($\beta_1 = 0.78$–0.8) [35,36]. Using Ising formalism, this type of transition is called ordinary transition; where this $J_s/J_b < 1$ relation is maintained [34]. The J_s and the J_b are the surface and bulk exchange parameter, respectively. The nature of the temperature dependence half-order spot intensity profile also suggests this $J_s/J_b < 1$ relation [37,34]. This relation also implies that the surface magnetic ordering temperature (T_s = 145 K) is force to follow the same value of the bulk magnetic ordering temperature (T_b), because of the influence of strong bulk field [34]. Thus, we also expect the enhancement of the bulk antiferromagnetic Néel temperature for this MnO/Ag(001) system than the bulk single crystal MnO. However, we can not use LEED as a probe for the bulk antiferromagnetic Néel temperature as it is only sensitive to the surface magnetism. Bulk sensitive techniques, like, Neutron diffraction experiment is needed for the further understanding of this aspect. For the NiO(001) single crystal, the nearly similar value of the critical exponent ($\beta = 0.89 \pm .01$) is reported by Kazumichi et al. [38]. We have also calculated the value of critical exponent for the case of 3 ML, where the obtained value is $\beta_1 = 0.16 \pm .03$ (see Fig. 5(b)).

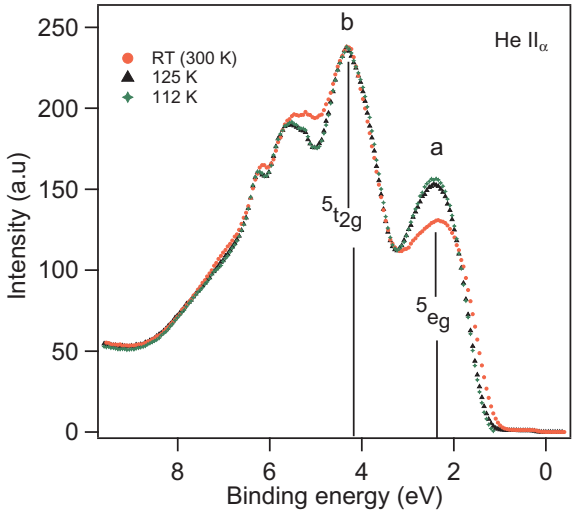

Fig. 6. Angle-resolved EDCs at $\bar{\Gamma}$ of 10 ML MnO film using He II$_\alpha$ (40.8 eV) photon energy for paramagnetic (300 K) and antiferromagnetic phase (110 K, 125 K).

This value of critical exponent falls in the range of 2D Ising model ($\beta = 0.125$) and special-transition of Ising system ($\beta_1 = 0.175$) [34]. This is also an expected behaviour as for the 3 ML case the properties of the film can not be completely reached to its bulk counterpart and the film should behave as a nearly 2D system.

3.2. Valence band electronic structure of MnO film

From the LEED study, we have already shown that there are different types of LEED structure arises in two different magnetic phases (PM and AFM) of MnO(001). Now, we will show how these magnetic structures affect the electronic structure of the material. Fig. 6 shows the variation of the EDCs for PM and AFM phase of 10 ML MnO(001) film grown on Ag(001). In Fig. 6, the origin of all the peaks can be well-explained using ligand field theory combined with configuration-interaction (CI) cluster approach [31]. Photoemission initial state of Mn^{2+} ($3d^5$) ion has $^6A_{1g}$ symmetry and after removing one 3*d* electron from t_{2g} or e_g, the photoemission final state is $^5t_{2g}$ and ^5e_g symmetry. But the real final state is a mixture of Mn 3*d*-hole and O 2*p*-hole (d^4-$d^5\underline{L}$) states, so in addition to the $^5t_{2g}$ and ^5e_g final states, there are also $^7t_{2g}$ and ^7e_g states. Because we have $d^6\underline{L}$ state (due to the transfer of the sixth '*d*' electron from ligand to the Mn^{2+} ion) mixed to the ground state and after photoionization of the sixth '*d*' electron, leaving behind a $d^5\underline{L}$ will be the final state which has $^7t_{2g}$ and ^7e_g symmetry states. The peaks 'a' and

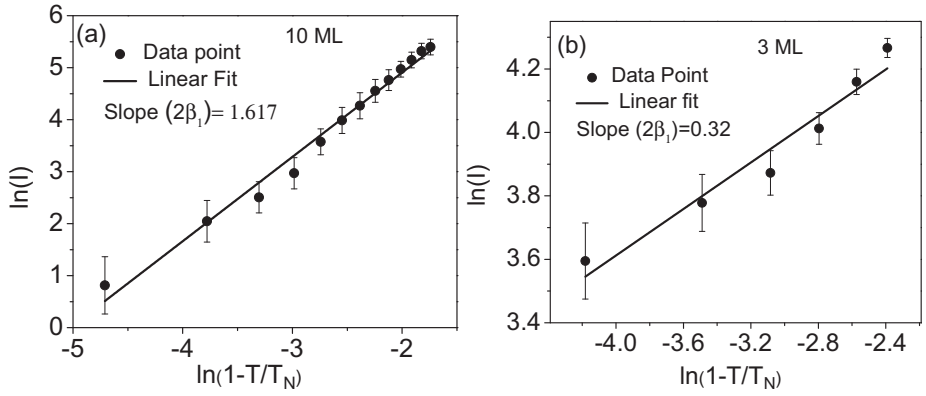

Fig. 5. ln(I) *vs.* ln(1-T/T_N) plot for the 10 ML (a) and 3 ML (b) MnO films, respectively. 'I' is the half-order spot intensity (Debye–Waller corrected). The critical exponent obtained from the linear fits are $\beta_1 = 0.81 \pm .03$ and $\beta_1 = 0.16 \pm .03$ for 10 ML and 3 ML films, respectively. The large error bar near the transition temperature is due to the very weak signal/background ratio, making difficulties for finding the exact value of spot intensity.

'b' in Fig. 6, is mainly the ^5e_g and $^5t_{2g}$ state. The other peaks in the spectra arises due to the hybridization of O 2*p* with the $^7t_{2g}$ and ^7e_g states. Low temperature spectra (AFM phase) shows, the band edge shifts towards higher binding energy by ~150 meV, compared to the PM phase, indicating the AFM state is more insulating than PM state. Further, it is also observed that in the AFM phase, ^5e_g state is sharper than in the PM phase while no change has been observed for the $^5t_{2g}$ state. Hermsmeier et al. [39], has investigated the valence band EDCs of MnO (001), below and above T_N and shown that below T_N the valence band is broader than PM phase which is exactly opposite to our results. While they could not reach any conclusion to interpret their results. Our observation of band narrowing and sharper ^5e_g state in the AFM phase is consistent with the band structure calculation for the AFM-II phase of MnO using Augmented Spherical Wave (ASW) method by Terakura et al. [40]. They have predicted that the decrease of the '*dd*' hopping during the PM to AFM transition as the origin of the sharpening of ^5e_g state as well as the gap opening in the AFM phase. However, no big changes in the spectral features between AFM and PM phase have been found. This could be due to the presence of short-range antiferromagnetic ordering in the MnO films even at higher temperatures than its Néel temperature. The presence of short-range antiferromagnetic ordering for bulk MnO is already confirmed by neutron diffraction and SPPD experiments [17,41,42].

4. Conclusion

In summary, we have used LEED as a technique for the probe of surface antiferromagnetism and shown that Néel temperature of the film can be estimated from the intensity *vs.* temperature curve of the magnetic half order spots in LEED. In our experiments, half order spots have been observed due to the low energy exchange-scattered electrons from the MnO(001) surface with the periodicity of the magnetic unit cell of MnO. Observation of the half order spot at low electron beam energy (<40 eV), below a certain temperature, and its typical temperature dependence, confirms its antiferromagnetic origin. Variation of Néel temperature with film thickness has been discussed. The higher value of the obtained Néel temperature for the MnO ultrathin films than the bulk Néel temperature value has been well discussed by the combined effect of superexchange interaction, finite-size effects and image charge screening effect. The surface magnetic critical exponent (β_1) varies from $0.16 \pm .03$ to $0.81 \pm .03$, upon changing film thickness from 3 to 10 ML, indicates the transition from nearly 2D Ising system to 3D Ising/Heisenberg system. Our study also shows how the antiferromagnetic ordering affects the valence band electronic structure of MnO. Furthermore, we observed band narrowing effects and sharpening of ^5E_g state and opening a gap of 150 meV in the AFM phase than the PM phase, consistent with the reported band structure calculation for the AFM-II phase of MnO.

Acknowledgements

The Micro-Nano initiative program of the Department of Atomic Energy (DAE), Government of India, is acknowledged for generous funding and support. A. K. K acknowledges the receipt of a fellowship from the ICTP-TRIL Programme, Trieste, Italy.

References

[1] C.G. Shull, W. Strauser, E. Wollan, Phys. Rev. 83 (1951) 333.
[2] W. Roth, Phys. Rev. 111 (1958) 772.
[3] M. Lines, Phys. Rev. 139 (1965) A1304.
[4] V.E. Henrich, Rep. Prog. Phys. 48 (1985) 1481.
[5] H.-J. Freund, E. Umbach, Adsorption on ordered surfaces of ionic solids and thin films, Proceedings of the 106th WE-Heraeus Seminar, Bad Honnef, Germany, February 15–18, 1993, vol. 33, Springer Science & Business Media, 2013.
[6] F. Müller, R. De Masi, D. Reinicke, P. Steiner, S. Hüfner, K. Stöwe, Surf. Sci. 520 (2002) 158–172.
[7] V. Henrich, P. Cox, The Surface Science of Metal Oxides, Cambridge University Press, 1996.
[8] C. Gao, W. Wulfhekel, J. Kirschner, Phys. Rev. lett. 101 (2008) 267205.
[9] W. Wulfhekel, C. Gao, J. Phys.: Condens. Matter 22 (2010) 084021.
[10] K.S. Menon, S. Mandal, J. Das, T.O. Menteş, M.A. Niño, A. Locatelli, R. Belkhou, Phys. Rev. B 84 (2011) 132402.
[11] M. El-Batanouny, J. Phys.: Condens. Matter 14 (2002) 6281.
[12] P. Palmberg, R. DeWames, L. Vredevoe, Phys. Rev. Lett. 21 (1968) 682.
[13] J. Das, S. Biswas, A.K. Kundu, S. Narasimhan, K.S. Menon, Phys. Rev. B 91 (2015) 125435.
[14] J. Das, A.K. Kundu, K.S. Menon, Vacuum 112 (2015) 5–11.
[15] P. Palmberg, R. De Wames, L. Vredevoe, T. Wolfram, J. Appl. Phys 40 (1969) 1158–1163.
[16] M. Hanf, C. Krembel, D. Bolmont, G. Gewinner, Phys. Rev. B 68 (2003) 144419.
[17] B. Hermsmeier, J. Osterwalder, D. Friedman, C. Fadley, Phys. Rev. lett. 62 (1989) 478.
[18] G. Rizzi, M. Petukhov, M. Sambi, R. Zanoni, L. Perriello, G. Granozzi, Surf. Sci. 482 (2001) 1474–1480.
[19] C. Hagendorf, S. Sachert, B. Bochmann, K. Kostov, W. Widdra, Phys. Rev. B 77 (2008) 075406.
[20] F. Li, G. Parteder, F. Allegretti, C. Franchini, R. Podloucky, S. Surnev, F. Netzer, J. Phys.: Condens. Matter 21 (2009) 134008.
[21] M. Nagel, I. Biswas, H. Peisert, T. Chassé, Surf. Sci. 601 (2007) 4484–4487.
[22] F. Müller, R. De Masi, P. Steiner, D. Reinicke, M. Stadtfeld, S. Hüfner, Surf. Sci. 459 (2000) 161–172.
[23] K. Marre, H. Neddermeyer, Surf. Sci. 287 (1993) 995–999.
[24] M. Bäumer, D. Cappus, H. Kuhlenbeck, H.-J. Freund, G. Wilhelmi, A. Brodde, H. Neddermeye, Surf. Sci. 253 (1991) 116–128.
[25] A.K. Kundu, K.S. Menon, J. Cryst. Growth 446 (2016) 85–91.
[26] A.K. Kundu, S. Barman, K.S. Menon, Phys. Rev. B 96 (2017) 195116.
[27] S. Mahatha, K.S. Menon, Curr. Sci. 98 (2010) 759.
[28] I. Blech, B. Averbach, Phys. Rev. 142 (1966) 287.
[29] K. Hayakawa, K. Namikawa, S. Miyake, J. Phys. Soc. Jpn. 31 (1971) 1408–1417.
[30] J. Das, K.S. Menon, J. Magn. Magn. Mater. 449 (2018) 415–422.
[31] J. Van Elp, R. Potze, H. Eskes, R. Berger, G. Sawatzky, Phys. Rev. B 44 (1991) 1530.
[32] M.-C. Desjonqueres, D. Spanjaard, Concepts in Surface Physics, Springer-Verlag, Berlin, 1993.
[33] S. Altieri, M. Finazzi, H. Hsieh, M. Haverkort, H.-J. Lin, C. Chen, S. Frabboni, G. Gazzadi, A. Rota, S. Valeri, et al., Phys. Rev. B 79 (2009) 174431.
[34] M. Marynowski, W. Franzen, M. El-Batanouny, V. Staemmler, Phys. Rev. B 60 (1999) 6053.
[35] D. Landau, K. Binder, Phys. Rev. B 41 (1990) 4633.
[36] H. Diehl, M. Shpot, Phys. rev. lett. 73 (1994) 3431.
[37] P. Palmberg, R. De Wames, L. Vredevoe, T. Wolfram, J. App. Phys. 40 (1969) 1158–1163.
[38] K. Namikawa, J. Phys. Soc. Jpn. 44 (1978) 165–171.
[39] B. Hermsmeier, J. Osterwalder, D. Friedman, B. Sinkovic, T. Tran, C. Fadley, Phys. Rev. B 42 (1990) 11895.
[40] K. Terakura, T. Oguchi, A. Williams, J. Kübler, Phys. Rev. B 30 (1984) 4734.
[41] A. Renninger, S. Moss, B. Averbach, Phys. Rev. 147 (1966) 418.
[42] Z.-X. Shen, J. Allen, P. Lindberg, D. Dessau, B. Wells, A. Borg, W. Ellis, J. Kang, S.-J. Oh, I. Lindau, et al., Phys. Rev. B 42 (1990) 1817.